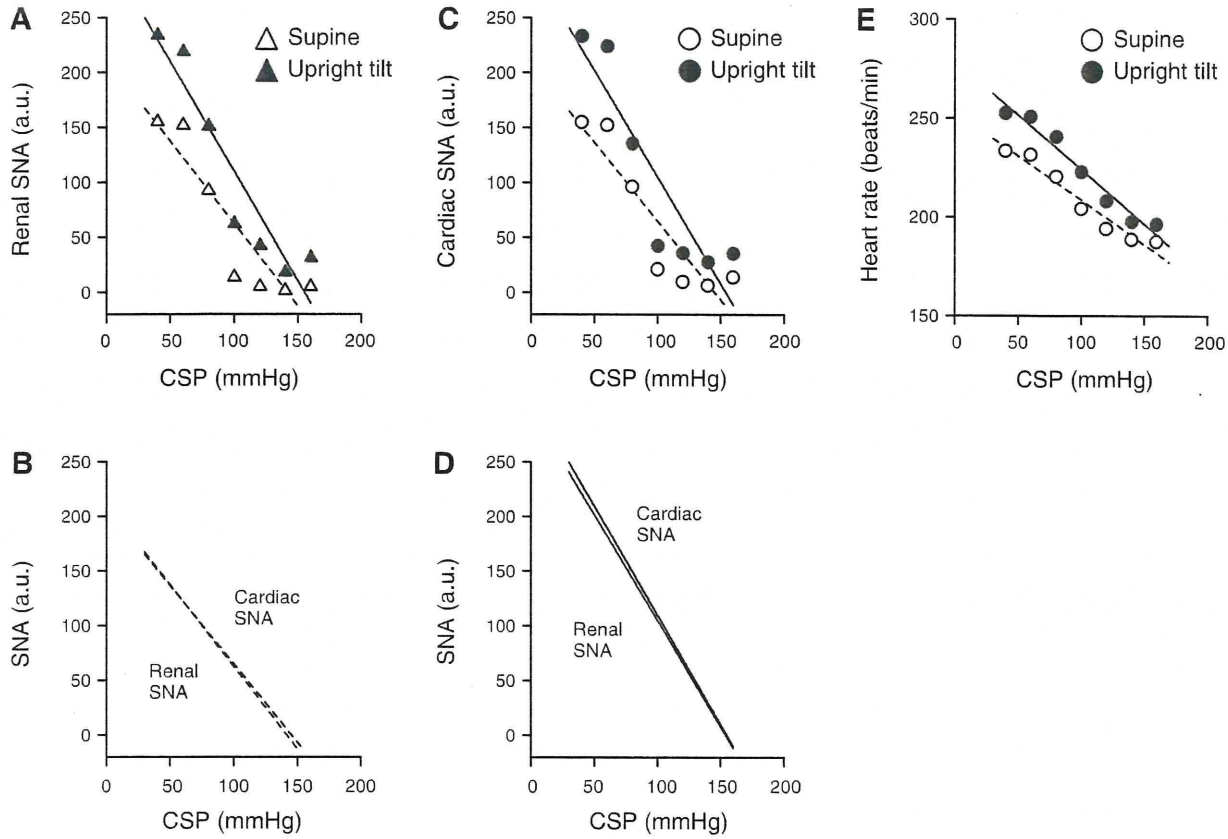

Fig. 4. Example of a model of the data shown in Fig. 2 using a simple regression line. Dotted and solid lines show the data in the supine and 60° upright tilt postures, respectively. The upright tilt shifted the baroreflex lines to a higher SNA similarly in renal (*A*) and cardiac SNAs (*C*). The lines were superimposed between these SNAs in the supine (*B*) and upright tilt postures (*D*). The upright tilt also shifted the baroreflex line of HR upward (*E*).

Baroreflex control of HR. In the representative time-series data, HR decreased in response to a stepwise increase in CSP in the 0° supine posture (Fig. 1*A*) and during 60° upright tilt (Fig. 1*B*). The upright tilt shifted the CSP-HR relationship upward to a higher HR (Fig. 2*E*), although HR was averaged for the last 10 s of each CSP level to investigate the steady-state, not transient, response to stepwise change in CSP.

Averaged data from all animals showed that the upright tilt shifted the CSP-HR relationship upward to a higher HR (Fig. 5*E*). When the static relationship between CSP and HR was fitted to a nonlinear reverse-sigmoidal curve (Fig. 6*E*), the P_1 (the range of HR response to CSP) and the maximal gain (at the midpoint of the logistic function) were larger at upright tilt than in the supine posture (Table 2), whereas P_2 (the coefficient of gain), P_3 (the midpoint CSP of the logistic function), and P_4 (the minimum value of HR) were not different between postures (Table 2). When the static relationship between CSP and HR was fitted to a linear regression line (Fig. 8*E*), the upright tilt increased the slope of regression from 0.46 ± 0.3 to 0.60 ± 0.3 beats·min^{-1}·mmHg^{-1}. The upright tilt increased operating HR (steady-state HR; 204 ± 11 beats/min in supine posture, 220 ± 12 beats/min in upright tilt posture).

DISCUSSION

Arterial baroreflex control of SNA is considered to have an important role to maintain AP under orthostatic stress against gravitational fluid shift directed toward the lower part of the body (15). In addition, we (8) recently reported that upright tilt resets arterial baroreflex control of renal SNA to increase orthostatic sympathetic activation. However, it remains unknown whether upright tilt resets arterial baroreflex control of SNA innervating to cardiovascular organs (i.e., the heart) other than the kidney. One major new finding in this study is that 60° upright tilt resets arterial baroreflex control of SNA to higher SNA similarly in renal and cardiac SNAs. This supports our hypothesis that upright tilt causes a parallel resetting of arterial baroreflex control of renal and cardiac SNAs in anesthetized rabbits.

Some regional differences between renal and cardiac SNAs certainly have been reported under some physiological conditions. First, for example, the dynamic high-pass characteristics in baroreflex control of SNA were greater in cardiac SNA than renal SNA (6, 10). Second, activating left atrial receptors increased cardiac SNA but decreased renal SNA (9). Last, hypoxia reset the AP-SNA relationship to higher AP and SNA in renal SNA but to lower AP and SNA in cardiac SNA (4). These lines of evidence indicate that renal and cardiac SNAs respond differently to specific physiological stimulation and stress (14).

However, our results indicate that upright posture induces a parallel resetting in arterial baroreflex control of renal and cardiac SNAs in the static characteristics. In agreement with previous studies (6, 7), the CSP-renal SNA reverse-sigmoidal curve was superimposable to the CSP-cardiac SNA curve in

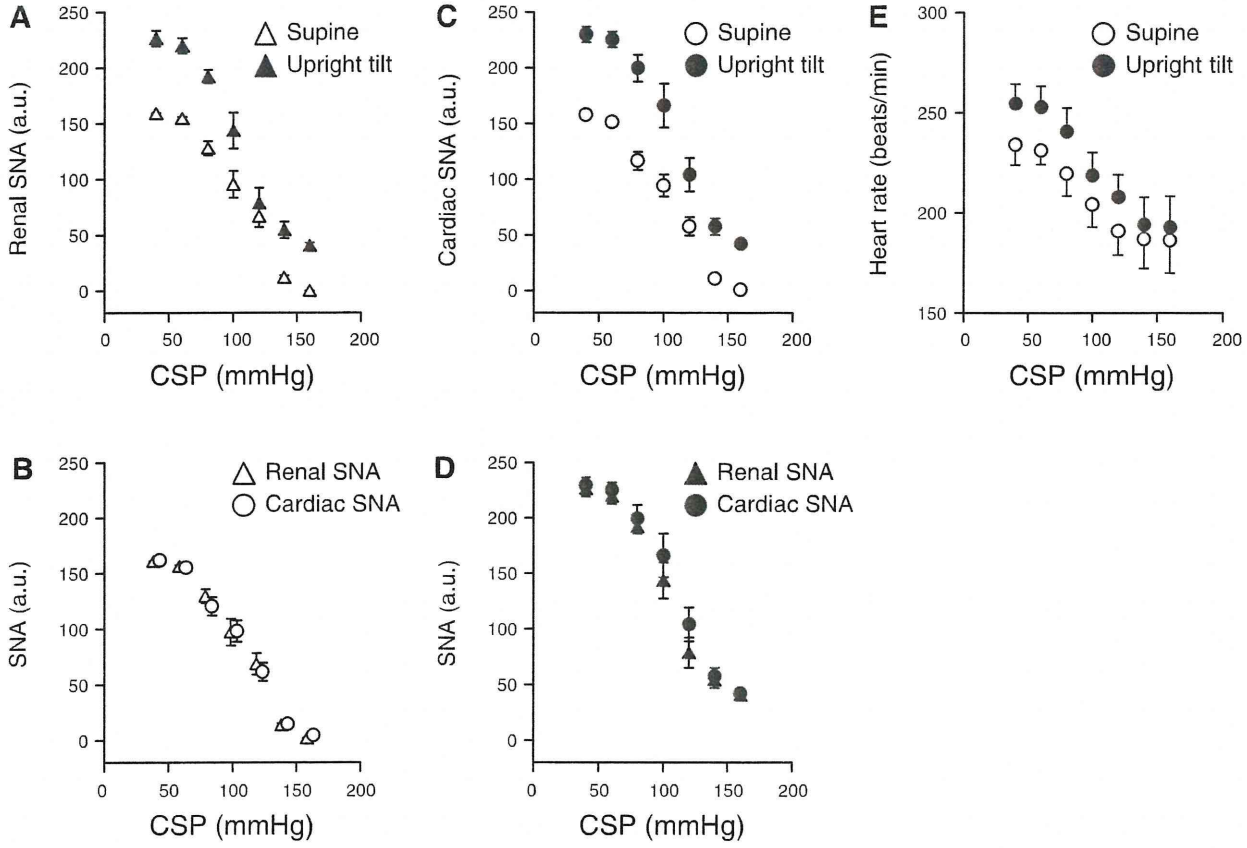

Fig. 5. Averaged data of arterial baroreflex control of renal (*A*) and cardiac SNAs (*C*) and HR (*E*) from all animals (n = 8). Open and filled symbols show the data in the supine and 60° upright tilt postures, respectively. The upright tilt shifted the baroreflex control of SNA to a higher SNA similarly in the CSP-renal SNA (*A*) and CSP-cardiac SNA relationships (*C*). *B* and *D* represent the superimposing of baroreflex control of SNA between renal and cardiac SNAs in both the supine and upright tilt postures, respectively. The upright tilt also shifted the baroreflex control of HR upward (*E*). Data are means ± SD.

the supine posture. This indicates that static nonlinear characteristics in arterial baroreflex control of renal SNA matched those of cardiac SNA in the posture. In addition, since upright tilt posture shifted the CSP-SNA curves upward similarly in renal and cardiac SNAs, the static nonlinear characteristics in arterial baroreflex control of renal SNA also matched those of cardiac SNA in upright tilt posture. These results were consistent with the close correlation between renal and cardiac SNAs during forced CSP changes with supine and upright tilt postures. They might also be consistent with a numerical simulation study indicating parallel responses of renal and cardiac SNAs to physiological pressure perturbations (AP change) (6).

Our results indicate that upright posture resets arterial baroreflex control of HR to a higher HR. This is consistent with the results of baroreflex resetting for cardiac SNA under upright tilt, because the P_I (the response range) and the maximal gain (at the midpoint of the logistic function) were larger in both CSP-HR and CSP-cardiac SNA relationships. The parallelism suggests that cardiac sympathetic efferent was a dominant determinant for HR in the present experimental condition with cutting of vagal nerves. Our results could be consistent with the increase in the baroreflex gain for HR assessed by a neck pressure/suction device in humans (11).

Limitations. The present study has several limitations. First, we excluded the efferent effect of vagally mediated arterial baroreflex and an anesthetic agent that could affect baroreflex control of SNA. Second, the vascular isolation of carotid sinus might decrease brain blood flow under, in particular, upright tilt position. Third, we eliminated cardiopulmonary baroreflex by cutting bilateral vagal nerves. Earlier human studies have indicated that nonhypotensive hypovolemic perturbations do not change AP but reduce central venous, right heart, and pulmonary pressures and cause vasoconstriction. These observations have been interpreted as reflexes triggered by cardiopulmonary baroreceptors (5, 12). However, Taylor et al. (17) showed that small reductions of effective blood volume reduce aortic baroreceptive areas and trigger hemodynamic adjustments that are so efficient that alterations in AP escape detection by conventional means. In addition, Fu et al. (2) reported that arterial baroreceptors are consistently unloaded during low levels (i.e., −10 and −15 mmHg) of lower body negative pressure in humans. Accordingly, further studies are needed to understand the relative importance and mutual cooperation of arterial and cardiopulmonary baroreflexes in AP control during orthostatic stress. Fourth, we investigated arterial baroreflex during upright posture in rabbits, which are quadripeds. However, denervation of both carotid and aortic arterial baroreflexes caused postural hypotension of ~50 mmHg during 60° upright tilt in quadripeds [rabbits and rats (16)]. This suggests that even in quadripeds, arterial baroreflex has a very important role in maintenance of AP under orthostatic stress.

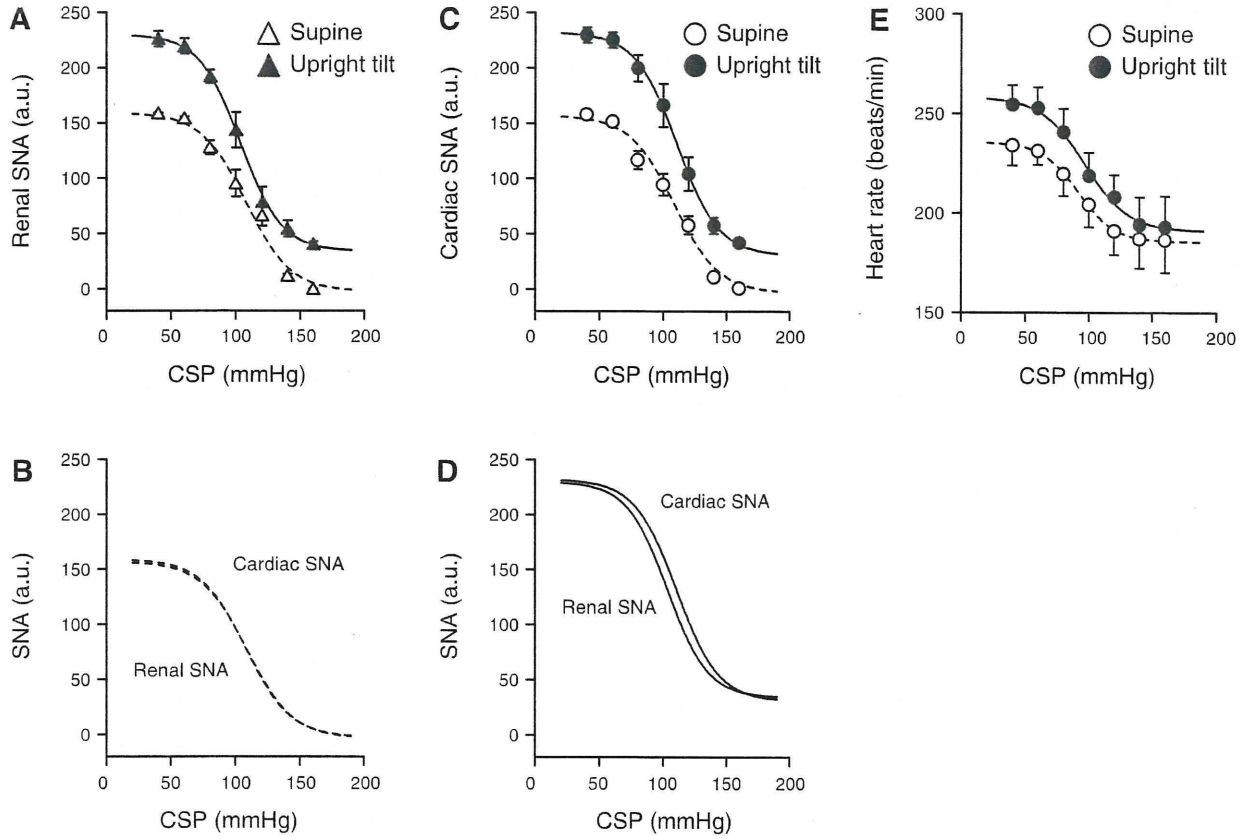

Fig. 6. A model of the averaged data shown in Fig. 5 using reverse-sigmoid 4-parameter logistic functions. Dotted and solid curves show the data in the supine and 60° upright tilt postures, respectively. The upright tilt shifted the baroreflex curves to a higher SNA similarly in renal (*A*) and cardiac SNAs (*C*). The curves were superimposed between these SNAs in the supine (*B*) and upright tilt postures (*D*). The upright tilt also shifted the baroreflex curve of HR upward (*E*).

Last, although we used two widely used traditional models to analyze the relationship between CSP and SNA, both have limited abilities to reproduce actual data. The nonlinear reverse-sigmoidal curve parameterized by a four-parameter logistic equation model provided high r^2 values (0.92–0.97) regardless of SNA type and posture. However, we failed to observe a saturation of SNA at the lowest CSP level in some cases (40 mmHg; Fig. 3, *A* and *B*, in upright tilt position). Lots of earlier studies have applied the model to AP and SNA (or HR) data under pharmacological perturbation (i.e., nitroprusside, phenylephrine) (1, 14), although it is difficult to observe clear saturation and/or threshold in the data. In contrary, the simple linear regression line model provided lower r^2 values (0.80–0.89). The plotted data did not appear to lie on a simple line in individuals (Fig. 4). Accordingly, we cannot conclude whether the relation between CSP and SNA is sigmoid or not. This problem is not the purpose of this study. Importantly, without modeling, our data (Fig. 2 and 5) indicate the parallel resetting of arterial baroreflex control of renal and cardiac SNAs.

Table 1. *Effect of upright tilt on parameters of baroreflex control of renal and catdiac SNAs*

	Supine	Upright tilt
Renal SNA		
P_1, a.u.	161 ± 2	196 ± 5*
P_2, a.u./mmHg	0.08 ± 0.01	0.08 ± 0.02
P_3, mmHg	105 ± 6	104 ± 6
P_4, a.u.	2 ± 1	34 ± 6*
G_{max}, a.u./mmHg	−1.5 ± 0.4	−1.9 ± 0.4*
Cardiac SNA		
P_1, a.u.	160 ± 2	201 ± 5*
P_2, a.u./mmHg	0.08 ± 0.01	0.08 ± 0.02
P_3, mmHg	109 ± 6	111 ± 6
P_4, a.u.	2 ± 1	31 ± 6*
G_{max}, a.u./mmHg	−1.4 ± 0.4	−1.9 ± 0.4*

Values are means ± SD (n = 8) for the parameters of baroreflex control of renal and cardiac sympathetic nerve activities (SNAs). See *Eq. 1* in METHODS for definitions of the 4 parameters of the logistic function. *P < 0.05, supine vs. upright tilt.

In conclusion, upright posture causes a resetting in arterial baroreflex control of SNA in parallel in renal and cardiac SNAs in anesthetized rabbits.

GRANTS

This study was supported by a research project promoted by the Ministry of Health, Labour and Welfare in Japan (no. H18-nano-ippan-003, H21-nano-ippan-005), a Grant-in-Aid for Scientific Research promoted by the Ministry of Education, Culture, Sports, Science and Technology in Japan (no. 20390462), and the Industrial Technology Research Grant Program from the New Energy and Industrial Technology Development Organization (NEDO) of Japan.

DISCLOSURES

No conflicts of interest, financial or otherwise, are declared by the author(s).

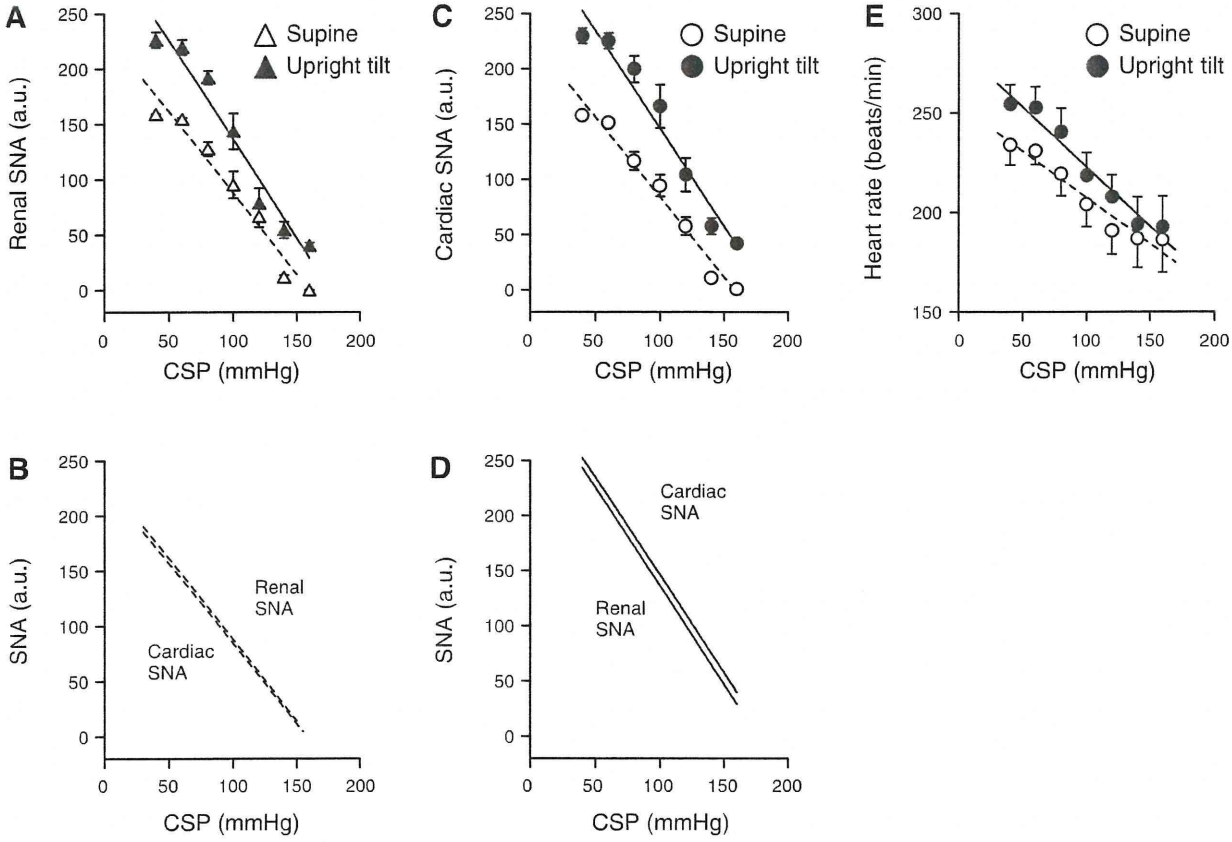

Fig. 7. A model of the averaged data shown in Fig. 5 using a simple regression line. Dotted and solid lines show the data in the supine and 60° upright tilt postures, respectively. The upright tilt shifted the baroreflex lines to a higher SNA similarly in renal (*A*) and cardiac SNAs (*C*). The lines were superimposed between these SNAs in the supine (*B*) and upright tilt postures (*D*). The upright tilt also shifted the baroreflex line of HR upward (*E*).

REFERENCES

1. **Eckberg DL, Sleight P.** *Human Baroreflexes in Health and Disease*. New York: Oxford Univ. Press, 1992, p. 3–299.
2. **Fu Q, Shibata S, Hastings JL, Prasad A, Palmer MD, Levine BD.** Evidence for unloading arterial baroreceptors during low levels of lower body negative pressure in humans. *Am J Physiol Heart Circ Physiol* 296: H480–H488, 2009.
3. **Glantz SA.** *Primer of Biostatistics* (4th ed.). New York: McGraw-Hill, 1997.
4. **Iriki M, Dorward P, Korner PI.** Baroreflex "resetting" by arterial hypoxia in the renal and cardiac sympathetic nerves of the rabbit. *Pflügers Arch* 370: 1–7, 1977.
5. **Johnson JM, Rowell LB, Niederberger M, Eisman MM.** Human splanchnic and forearm vasoconstrictor responses to reductions of right atrial and aortic pressures. *Circ Res* 34: 515–524, 1974.
6. **Kamiya A, Kawada T, Yamamoto K, Michikami D, Ariumi H, Miyamoto T, Shimizu S, Uemura K, Aiba T, Sunagawa K, Sugimachi M.** Dynamic and static baroreflex control of muscle sympathetic nerve activity (SNA) parallels that of renal and cardiac SNA during physiological change in pressure. *Am J Physiol Heart Circ Physiol* 289: H2641–H2648, 2005.
7. **Kamiya A, Kawada T, Yamamoto K, Michikami D, Ariumi H, Miyamoto T, Uemura K, Sugimachi M, Sunagawa K.** Muscle sympathetic nerve activity averaged over 1 min parallels renal and cardiac sympathetic nerve activity in response to a forced baroreceptor pressure change. *Circulation* 112: 384–386, 2005.
8. **Kamiya A, Kawada T, Yamamoto K, Michikami D, Ariumi H, Uemura K, Zheng C, Shimizu S, Aiba T, Miyamoto T, Sugimachi M, Sunagawa K.** Resetting of the arterial baroreflex increases orthostatic sympathetic activation and prevents postural hypotension in rabbits. *J Physiol* 566: 237–246, 2005.
9. **Karim F, Kidd C, Malpus CM, Penna PE.** The effects of stimulation of the left atrial receptors on sympathetic efferent nerve activity. *J Physiol* 227: 243–260, 1972.
10. **Kawada T, Shishido T, Inagaki M, Tatewaki T, Zheng C, Yanagiya Y, Sugimachi M, Sunagawa K.** Differential dynamic baroreflex regulation of cardiac and renal sympathetic nerve activities. *Am J Physiol Heart Circ Physiol* 280: H1581–H1590, 2001.
11. **Ogoh S, Yoshiga CC, Secher NH, Raven PB.** Carotid-cardiac baroreflex function does not influence blood pressure regulation during head-up tilt in humans. *J Physiol Sci* 56: 227–233, 2006.
12. **Pawelczyk JA, Raven PB.** Reductions in central venous pressure improve carotid baroreflex responses in conscious men. *Am J Physiol Heart Circ Physiol* 257: H1389–H1395, 1989.
13. **Persson P, Kirchheim H.** *Baroreceptor Reflexes: Integrative Functions and Clinical Aspects*. Berlin: Springer, 1991.
14. **Ramchandra R, Hood SG, Denton DA, Woods RL, McKinley MJ, McAllen RM, May CN.** Basis for the preferential activation of cardiac sympathetic nerve activity in heart failure. *Proc Natl Acad Sci USA* 106: 924–928, 2009.
15. **Rowell LB.** *Human Cardiovascular Control*. New York: Oxford Univ. Press, 1993, p. 3–254.
16. **Sato T, Kawada T, Sugimachi M, Sunagawa K.** Bionic technology revitalizes native baroreflex function in rats with baroreflex failure. *Circulation* 106: 730–734, 2002.
17. **Taylor JA, Halliwill JR, Brown TE, Hayano J, Eckberg DL.** "Non-hypotensive" hypovolaemia reduces ascending aortic dimensions in humans. *J Physiol* 483: 289–298, 1995.

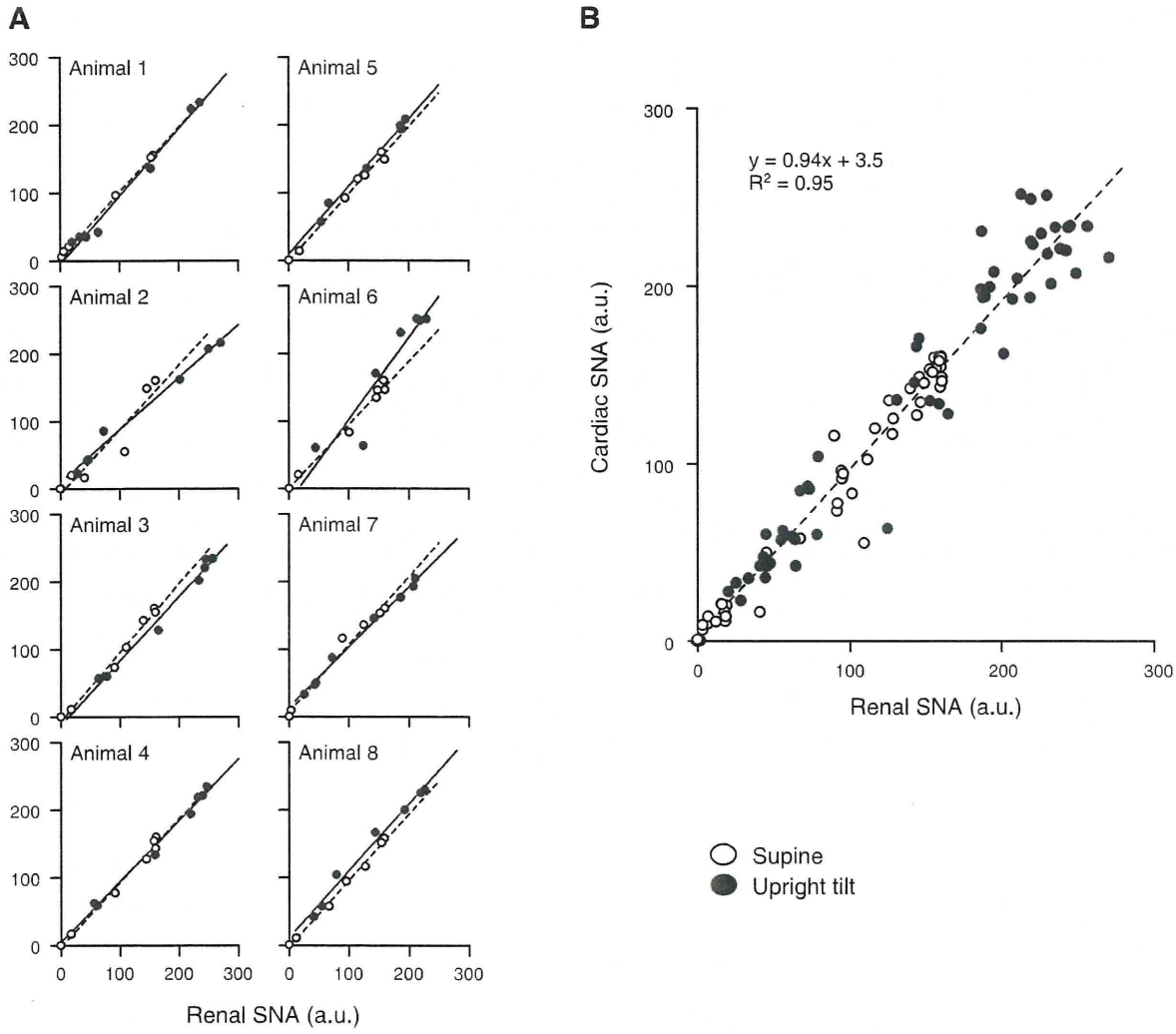

Fig. 8. Scatter plots and regression lines drawn between renal and cardiac SNAs in supine (dotted lines) and upright tilt postures (solid lines) during stepwise changes in CSP for each subject (*A*) and the pooled data from all 8 subjects (*B*).

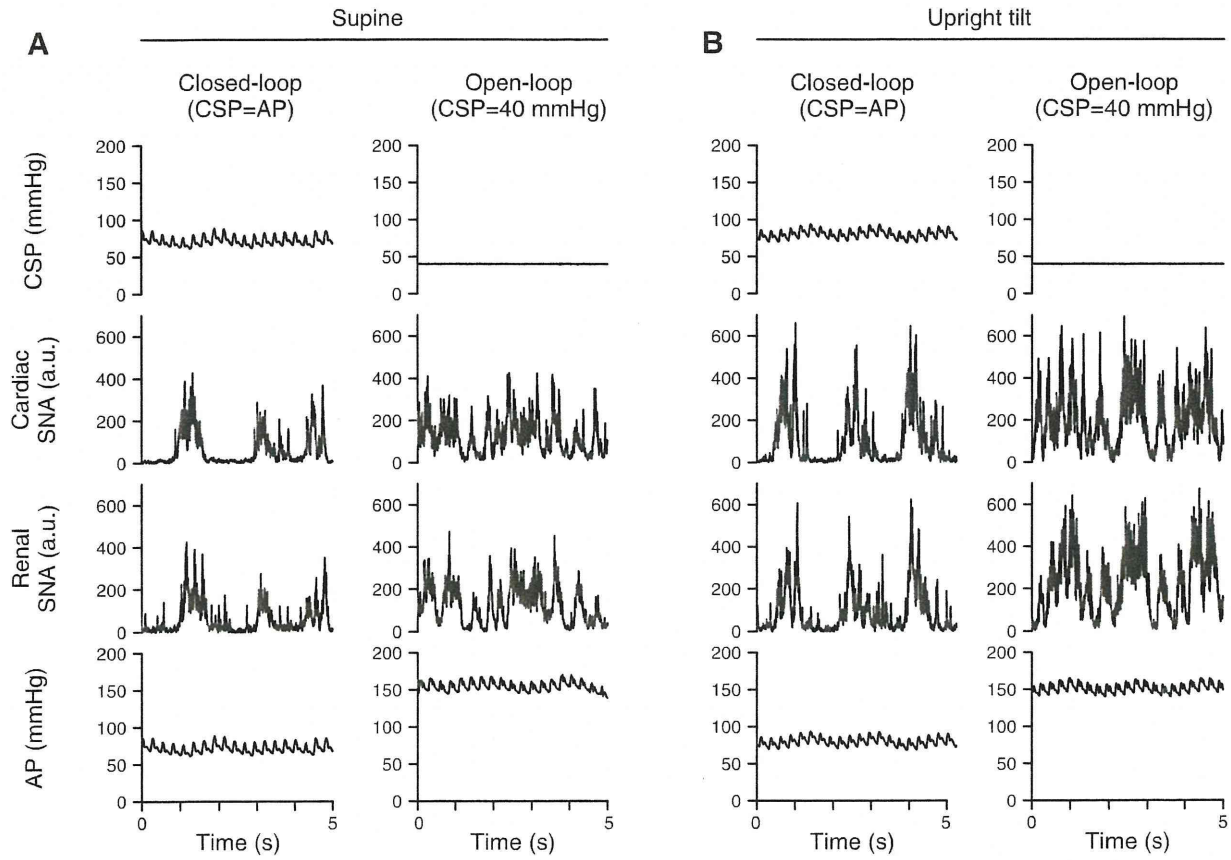

Fig. 9. Discharge characteristics of the renal and cardiac SNAs in supine (*A*) and 60° upright tilt postures (*B*) under the baroreflex closed-loop condition, where CSP was artificially matched with systemic AP, and under the open-loop condition, where CSP was fixed at 40 mmHg. Variables were resampled at 200 Hz. Data were obtained from the same animal studied in Fig. 1.

Table 2. *Effect of upright tilt on parameters of baroreflex control of HR*

	Supine	Upright tilt
P_1, beats/min	53 ± 11	67 ± 11*
P_2, beats·min^{-1}·mmHg^{-1}	0.07 ± 0.03	0.07 ± 0.03
P_3, mmHg	93 ± 8	97 ± 12
P_4, beats/min	184 ± 17	191 ± 18
G_{max}, beats·min^{-1}·mmHg^{-1}	−0.9 ± 0.2	−1.2 ± 0.4*

Values are means ± SD (n = 8) for the parameters of baroreflex control of heart rate (HR). *$P < 0.05$, supine vs. upright tilt.

J Physiol Sci (2010) 60:205–212
DOI 10.1007/s12576-010-0086-y

ORIGINAL PAPER

Right ventricular stiffness constant as a predictor of postoperative hemodynamics in patients with hypoplastic right ventricle: a theoretical analysis

Shuji Shimizu · Toshiaki Shishido · Dai Une · Atsunori Kamiya · Toru Kawada · Shunji Sano · Masaru Sugimachi

Received: 9 December 2009 / Accepted: 10 January 2010 / Published online: 4 February 2010

Abstract One and a half ventricle repair (1.5VR) is a surgical option for hypoplastic right ventricle (RV). The benefits of this procedure compared to biventricular repair (2VR) or Fontan operation remain unsettled. To compare postoperative hemodynamics, we performed a theoretical analysis using a computational model based on lumped-parameter state-variable equations. We varied the RV stiffness constant (B_{RV}) to simulate the various RV hypoplasia, and estimated hemodynamics for a given B_{RV}. With $B_{RV} < 150\%$ of normal, cardiac output was the largest in 2VR. With $B_{RV} > 150\%$, cardiac output became larger in 1.5VR than in 2VR. With $B_{RV} > 250\%$, RV end-diastolic volume was almost the same between 1.5VR and 2VR, and a rapid increase in atrial pressure precluded the use of 1.5VR. These results indicate that the beneficial effect of 1.5VR depends on the RV stiffness constant. Determination of management strategy should not only be based on the morphologic parameters but also on the physiological properties of RV.

S. Shimizu (✉) · T. Shishido · D. Une · A. Kamiya · T. Kawada · M. Sugimachi
Department of Cardiovascular Dynamics, Advanced Medical Engineering Center, National Cardiovascular Center Research Institute, 5-7-1 Fujishiro-dai, Suita, Osaka 565-8565, Japan
e-mail: shujismz@ri.ncvc.go.jp

S. Shimizu · S. Sano
Department of Cardiovascular Surgery, Okayama University Graduate School of Medicine, Dentistry and Pharmaceutical Sciences, Okayama, Japan

S. Shimizu
Japan Association for the Advancement of Medical Equipment, Tokyo, Japan

Keywords One and a half ventricle repair · Right ventricular stiffness · Hypoplastic right ventricle · Computational model

Introduction

One and a half ventricle repair (1.5VR) is a surgical option for hypoplastic right ventricle (RV) caused by various congenital heart diseases including pulmonary atresia with intact ventricular septum (PA/IVS), Ebstein's anomaly or their relatives. In this procedure, the superior vena cava (SVC) is directly connected to the pulmonary artery (PA). Therefore, the blood from SVC directly enters PA, whereas the blood from the inferior vena cava (IVC) is pumped by RV to PA. This procedure is clinically acceptable because of its low surgical risk [1, 2]. However, the benefits of this procedure on postoperative hemodynamics in patients with a wide spectrum of RV hypoplasia compared to other procedures such as biventricular repair (2VR) and Fontan operation remain unsettled [3]. Furthermore, conversion to Fontan circulation was required late after 1.5VR in a possibly inappropriate candidate [4].

Although various authors reported an arbitrary selection scheme for the procedures based on RV morphology such as RV end-diastolic volume (RVEDV) [1, 2, 5], the long-term outcomes of 1.5VR have remained insufficiently known [5]. The previous criteria do not likely predict postoperative hemodynamics of these complex circulations accurately because morphological values measured preoperatively largely depend on the RV preload and afterload conditions, which change remarkably between subjects and between before and after the operation.

Hypoplastic RV is physiologically characterized by increased RV stiffness, caused by hypertrophy and

fibroelastosis of RV muscles [6]. However, how RV stiffness influences the postoperative hemodynamics has not been reported. Given the small number of patients with each of the wide variety of preoperative RV conditions [7, 8], the influence of RV stiffness on 1.5VR, 2VR, and Fontan operation cannot be examined by clinical study. It is also difficult to experimentally reproduce hemodynamics before and after 1.5VR for hypoplastic RV with various stiffness. In view of the above, we attempted to clarify postoperative hemodynamics by a theoretical analysis using a computational model based on lumped-parameter state-variable equations. The present results indicate that the RV stiffness constant may provide selection criteria for 1.5VR.

Materials and methods

The electrical analogs of the model used to simulate the cardiovascular system are shown in Fig. 1. We modeled the postoperative cardiovascular system mathematically by a combination of the time-varying elastance cardiac chamber model and the three-element Windkessel vascular model. We set the normal values of parameters to be appropriate for a 75-kg man. These values were obtained from the literature [9–13] and are listed in Table 1. Since the data of the pressure–volume relationship of the atrium were scarcely available, parameters of the atrium were surmised from the literature [10–12].

Heart

The right and left ventricular chambers as well as the atrial chambers are represented by the time-varying elastance model [9, 10, 13]. The end-systolic pressure–volume relationship is described by a linear formula:

$$P_{es.cc} = E_{es.cc}\left[V_{es.cc} - V_{0.cc}\right] \quad (1)$$

where $P_{es.cc}$ and $V_{es.cc}$ are end-systolic pressure and volume, respectively; $E_{es,cc}$ is the maximal volume elastance; $V_{0.cc}$ is the volume at which $P_{es,cc}$ is equal to 0 mmHg. cc denotes each chamber, i.e., RA for the right atrium, LA for the left atrium, RV for the right ventricle, or LV for the left ventricle. The end-diastolic pressure–volume relationship is represented by a non-linear formula:

$$P_{ed.cc} = A_{cc}\left[e^{B_{cc}(V_{ed.cc}-V_{0.cc})} - 1\right] \quad (2)$$

where $P_{ed.cc}$ and $V_{ed.cc}$ are end-diastolic pressure and volume, respectively; A_{cc} and B_{cc} are constants [9, 10, 13]. We assumed the time course of the time-varying elastance by defining normalized elastance curve $e_{cc}(t)$ as:

Table 1 Parameters used in modeling

Heart rate (HR), beats/min	75			
Duration of cardiac cycle (T_c), ms	800			
Time advance of atrial systole (DT), ms	16			
Total stressed blood volume (V_s), ml	750	(control only)		
	LV	RV	LA	RA
Time to end systole (T_{es}), ms	200	200	120	120
End-systolic elastance (E_{es}), mmHg/ml	3.0	0.7	0.5	0.5
Scaling factor of EDPVR (A), mmHg	0.35	0.35	0.06	0.06
Exponent scaling factor for EDPVR (B), ml^{-1}	0.033	0.023	0.264	0.264
Unstressed volume (V_0), ml	0	0	5	5
	Aortic	Pulmonary	Mitral	Tricuspid
Valvular resistance (forward), (mmHg s)/ml	0.001	0.001	0.001	0.001
	Systemic		Pulmonary (p)	
	Superior (ss)	Inferior (si)		
Arterial resistance (R_a), (mmHg s)/ml	2.25	1.5	0.03	
Characteristic impedance (R_c), (mmHg s)/ml	0.075	0.05	0.02	
Venous resistance (R_v), (mmHg s)/ml	0.0375	0.025	0.015	
Arterial capacitance (C_a), ml/mmHg	0.528	0.792	13	
Venous capacitance (C_v), ml/mmHg	28	42	8	

LV Left ventricle, *RV* right ventricle, *LA* left atrium, *RA* right atrium, *EDPVR* end-diastolic pressure–volume relationship

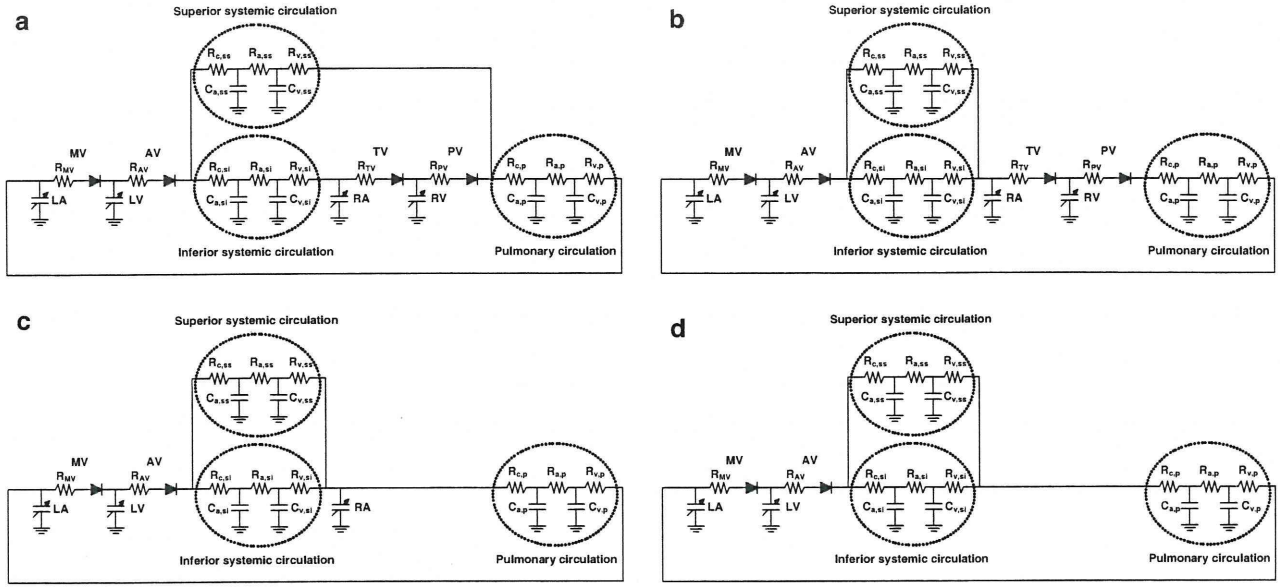

Fig. 1 **a** The electric equivalent circuit of one and a half ventricle repair. **b** Biventricular repair (normal circulation). **c**,**d** Variations of Fontan operation [**c** atriopulmonary connection (APC); **d** total cavopulmonary connection (TCPC)]. *LV* and *RV* left and right ventricles, *LA* and *RA* left and right atria, *AV* and *MV* aortic and mitral valves, *PV* and *TV* pulmonary and tricuspid valves, C_a and C_v lumped arterial and venous capacitances, R_c characteristic impedances. R_a lumped arterial resistances, R_v venous resistances, *ss* superior systemic circulation, *si* inferior systemic circulation, *p* pulmonary circulation

$$e_{cc}(t) = 0.5[1 - \cos(\pi t/T_{es.cc})] \ (0 \le t < 2T_{es.cc})$$
$$e_{cc}(t) = 0 \ (2T_{es.cc} \le t < T_c) \tag{3}$$

where t is the time from the start of systole, $T_{es.cc}$ is the duration of systole, and T_c is the duration of cardiac cycle. Using $e_{cc}(t)$, the instantaneous pressure, $P_{cc}(t)$, is described by:

$$P_{cc}(t) = [P_{es.cc}(V_{cc}) - P_{ed.cc}(V_{cc})]e_{cc}(t) + P_{ed.cc}(V_{cc}) \tag{4}$$

Ventricular systole is preceded by atrial systole. The time advance of atrial systole (DT) is calculated as the fixed fraction of T_c ($DT = 0.02T_c$). Function of each chamber is characterized by the parameters $E_{es.cc}$, $T_{es.cc}$, $V_{0.cc}$, A_{cc}, B_{cc}, and $e_{cc}(t)$. The same $e_{cc}(t)$ was used for all chambers, but the other parameters were different between chambers, as shown in Table 1.

Vascular system

Basically, the pulmonary and systemic circulations are modeled as modified Windkessel impedances. Each vascular system is modeled by lumped venous (C_v) and arterial (C_a) capacitances, a characteristic impedance (R_c) that is related to the stiffness of the proximal aorta or pulmonary artery, a lumped arterial resistance (R_a), and a resistance proximal to C_v (R_v). This framework is similar to that used in deriving Guyton's resistance to venous return [14].

To simulate the postoperative hemodynamics of 1.5VR, the systemic circulation is divided into two parts, the superior and the inferior circulation. Therefore, the parameters of the systemic circulation are also divided into the superior and inferior ones, as shown in Fig. 1. Blood flow in the descending aorta is reported to be 63.8% of the left ventricular output [15]. The compliance of the IVC is considered to be 66.6% of the total venous compliance [16]. Thus, in our model, arterial and venous compliances of the inferior systemic circulation are adjusted to 0.6 times those of the compliance of the total circulation, and the blood flow of the inferior systemic circulation is controlled to be 60% of the left ventricular output by adjusting the resistances of R_c, R_a, and R_v.

The capacitance of the superior systemic circulation is also divided into arterial ($C_{a.ss}$) and venous ($C_{v.ss}$). Similarly, arterial and venous capacitances are defined for the inferior systemic circulation ($C_{a.si}$ and $C_{v.si}$) and for the pulmonary circulation ($C_{a.p}$ and $C_{v.p}$). The ratio of C_a to C_v was obtained from the literature [9, 10, 13]. The relationship between pressure (P_c) and volume (V_c) in each capacitance is described by the following linear formula.

$$P_c = \frac{V_c}{C} \tag{5}$$

The changes in volume in each capacitance ($dV(t)/dt$) are described by the differential equations below

$$\frac{dV(t)}{dt} = \sum Q_{\text{in-flow}}(t) - \sum Q_{\text{out-flow}}(t) \quad (6)$$

where $\Sigma Q_{\text{in-flow}}(t)$ and $\Sigma Q_{\text{out-flow}}(t)$ indicate the sum of instantaneous volumetric flow rates at the inlet and outlet of each compartment, respectively. Each of the aortic, mitral, pulmonary, and tricuspid valves is described as an ideal diode with a serially connected small resistor.

In the 1.5VR model, the superior circulation flows from SVC to PA, while the inferior blood flow returns to RA through IVC as shown in Fig. 1a. The models of 2VR (Fig. 1b) and variations of Fontan operation [Fig. 1c, atriopulmonary connection (APC); Fig. 1d, total cavopulmonary connection (TCPC)] are constructed for comparisons. Although the superior and inferior systemic circulations return to RA in both 2VR and APC models, RA is directly connected to PA in the APC model. In the TCPC model, SVC and IVC are directly connected to PA. All parameter values were the same for all of these models except total stressed blood volume (see below) (Table 1).

Hypoplastic RV

Hypoplastic RV is physiologically characterized by an increase in RV stiffness caused by hypertrophy and fibroelastosis of RV muscles [6]. Recalling Eq. 2 for RV, we have:

$$P_{\text{ed.RV}} = A_{\text{RV}}\left[e^{B_{\text{RV}}\left(V_{\text{ed.RV}} - V_{0.\text{RV}}\right)} - 1\right] \quad (7)$$

where B_{RV} is stiffness constant of RV. The value of B_{RV} was changed stepwise from 0.023/ml (normal RV) to 0.143/ml (extremely stiff RV) in increments of 0.01/ml to simulate the various degrees of RV stiffness associated with hypoplasia (Fig. 2).

Protocols

First, the control state was simulated by the 2VR model with normal RV stiffness constant ($B_{\text{RV}} = 0.023$). The total stressed blood volume (V_s), equal to the sum of the stressed volumes in each capacitance and the volume of each chamber, was set as 750 ml to reproduce normal hemodynamics.

$$V_s = V_{\text{LV}} + V_{\text{RV}} + V_{\text{LA}} + V_{\text{RA}} + V_{\text{Ca.ss}} + V_{\text{Cv.ss}} + V_{\text{Ca.si}} + V_{\text{Cv.si}} + V_{\text{Ca.p}} + V_{\text{Cv.p}} \quad (8)$$

We solved these simultaneous equations (Eqs. 1–8) using the component ODE45 of MATLAB, based on the Runge–Kutta method (MathWorks). The hemodynamic parameters of 2VR with normal RV stiffness constant are listed in Table 2.

Next, systemic cardiac output, pulmonary arterial pressure (PAP), right atrial pressure (RAP), and RVEDV after each procedure were calculated for each RV stiffness constant. Heart rate was kept constant and mean systemic arterial pressure (MAP) was controlled at the same value as that of the control state, by adjusting the total stressed blood volume.

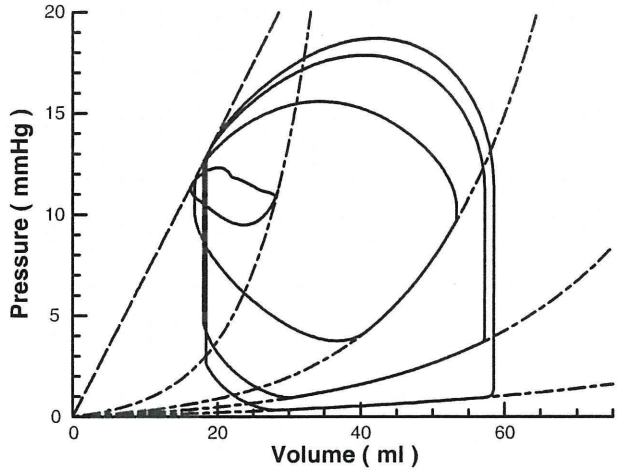

Fig. 2 Right ventricular pressure–volume loops (PV loop) after one and a half ventricle repair. With the increase in the right ventricular stiffness constant, the PV loop became smaller. The *horizontal axis* is the instantaneous right ventricular volume (ml) and the *longitudinal axis* is the instantaneous right ventricular pressure (mmHg)

Table 2 Control hemodynamic parameters (2VR with normal RV stiffness constant)

Parameter	Value
Heart rate (HR), beats/min	75
Mean systemic arterial pressure (MAP), mmHg	80.3
Mean pulmonary arterial pressure (PAP), mmHg	13.6
Mean right atrial pressure (RAP), mmHg	2.34
Mean left atrial pressure (LAP), mmHg	8.26
Left ventricular cardiac output (CO), l/min	4.95

Results

Figure 3a shows the impact of the RV stiffness constant on systemic cardiac output after each procedure. In the Fontan circulation (APC and TCPC), systemic cardiac output was independent of the RV stiffness constant and remained at 4.40 l/min. Under the condition of normal RV stiffness constant, systemic cardiac output was 4.95 l/min in 2VR and 4.73 l/min in 1.5VR, being 13 and 8% greater than that of Fontan circulation, respectively. As the RV stiffness constant was increased from the control value to mimic increased severity of RV

hypoplasia, systemic cardiac output decreased in both 2VR and 1.5VR circulations. Within the range between 100 and 150% of the control RV stiffness constant, systemic cardiac output of 2VR circulation was obviously greater than those of other two circulations. With the RV stiffness constant >150%, systemic cardiac output became greater in 1.5VR than in 2VR. In this situation, 2VR needed larger stressed blood volume than 1.5VR to maintain MAP (Fig. 3d).

The results for PAP and RAP are shown in Fig. 3b. As the RV stiffness constant increased, PAP decreased and RAP increased in both 2VR and 1.5VR circulations. In 2VR circulation, RAP increased steeply as the RV stiffness constant increased up to 150% of normal, and exceeded the atrial pressure of TCPC when the RV stiffness constant increased above 150% of normal. In 1.5VR circulation, RAP also increased but more slowly and exceeded the atrial pressure of TCPC only when the RV stiffness constant increased above 250% of normal. PAP in 1.5VR circulation, which was equal to SVC pressure, became higher than PAP in 2VR circulation in the range of RV stiffness constant >150% of normal.

In the control state, RVEDV in 2VR was 87.7 ml, which was treated as the value of 100% of RVEDV. The influence of the RV stiffness constant on RVEDV is shown in Fig. 3c. In 2VR circulation, RVEDV decreased as the RV stiffness constant increased. In 1.5VR circulation, RVEDV reduced only slightly with an increase in the RV stiffness constant until 250% of normal. In the range of RV stiffness constant >250% of normal, RVEDV showed a relatively linear decay in both 2VR and 1.5VR circulations, and there was no difference in RVEDV between 2VR and 1.5VR. In this situation, both 1.5VR and 2VR needed larger stressed blood volume than Fontan circulation (Fig. 3d).

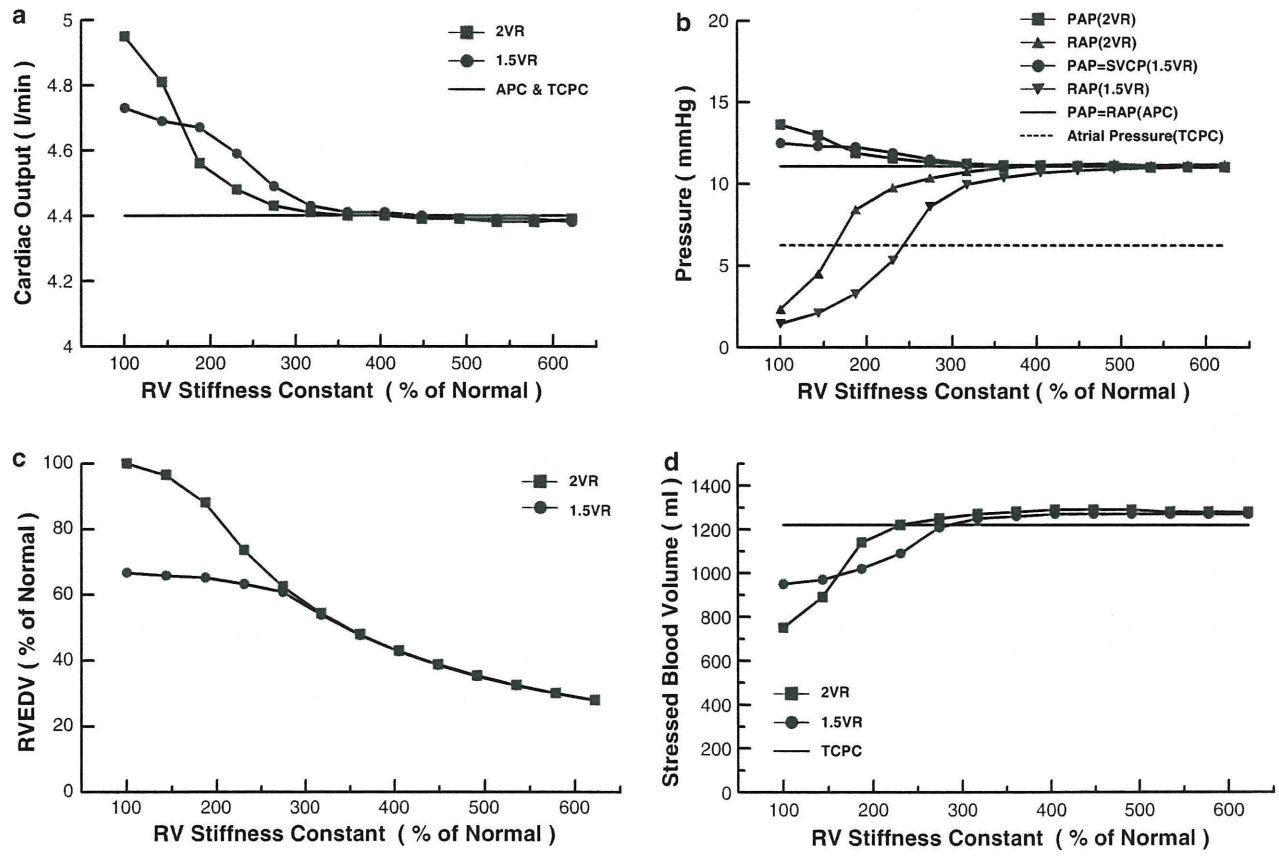

Fig. 3 **a** The relationship between systemic cardiac output (l/min) and % stiffness constant of hypoplastic right ventricle. The *horizontal axis* is the ratio of RV stiffness constant (% stiffness constant) to the normal value. **b** The relationship between pulmonary arterial pressure or right atrial pressure (mmHg) and % stiffness constant of hypoplastic RV. Pulmonary arterial pressure is the same as right atrial pressure in APC. **c** The relationship between % RVEDV and % stiffness constant of hypoplastic RV. **d** The relationship between stressed blood volume (ml) and % stiffness constant. *2VR* biventricular repair, *1.5VR* one and a half ventricle repair, *APC* and *TCPC* variations of Fontan operation (*APC* atriopulmonary connection, *TCPC* total cavopulmonary connection); *PAP* pulmonary arterial pressure, *RAP* right atrial pressure, *SVCP* superior vena caval pressure, *RVEDV* right ventricular end-diastolic volume

Discussion

The results of this theoretical analysis suggest that, in patients with hypoplastic RV, postoperative hemodynamics depends largely on the RV stiffness constant. PA/IVS, Ebstein's anomaly or their relatives are characterized by varying degrees of underdevelopment of RV. For a severely hypoplastic RV, the definitive treatment is single ventricular circulation. For a mildly hypoplastic RV, biventricular circulation is expected to have merit. Recently, 1.5VR has been proposed to reduce the surgical risk of 2VR. The use of 1.5VR has lowered the early or midterm mortality, and adequate growth of RV and the tricuspid valve has been documented in some patients [2]. However, the postoperative RV dysfunction or arrhythmic event has also been reported, in particular, when the patients are on the borderline of criteria between 1.5VR and Fontan operation [4, 5].

For the choice of surgical options among Fontan operation, 1.5VR, and 2VR, the previously used criteria were based on morphologic characteristics of the hypoplastic RV, such as RVEDV. However, simple anatomic indices may be inaccurate, since these values are dependent on the afterload and preload conditions. For that reason, the treatment strategy for hypoplastic RV based on the anatomic indices remains controversial. We focused on the intrinsic property of hypoplastic RV, i.e., RV stiffness constant. The fact that the RV stiffness constant, an index of chamber property, is relatively independent of the loading condition is important for the accurate prediction of postoperative hemodynamics. Based on the results of the present study, we propose that patients with hypoplastic RV can be classified into three groups according to the RV stiffness constant. The first group consists of patients with mild RV hypoplasia (RV stiffness constant <150% of normal), in whom enlargement of RV is expected after the operation. At the other extreme, the second group consists of patients with severe RV hypoplasia (RV stiffness constant >250%), in whom no RV reconstruction is expected to have merit. In addition, we have shown that there certainly exists a third group consisting of patients with intermediate RV hypoplasia (RV stiffness constant between 150 and 250%), who would benefit more from 1.5VR than from 2VR or Fontan operation.

Mild RV hypoplasia

When RV hypoplasia is mild (RV stiffness constant <150% of normal), systemic cardiac output is greater in 2VR than in 1.5VR or Fontan operation (APC or TAPC). Therefore, we recommend that 2VR should be chosen in the mild RV hypoplasia group. Although systemic cardiac output in 1.5VR is also greater than that in Fontan operation, SVC pressure (which is equal to PAP) is higher than that of APC. Accordingly, the upper part of the body is exposed to higher SVC pressure in 1.5VR, which may cause postoperative pleural effusion [2]. A large pressure gradient between SVC and IVC also results in abnormal venous collaterals from SVC to IVC [17–20], and they could effectively increase the venous return to RA in 1.5VR.

Intermediate RV hypoplasia

When RV hypoplasia is intermediate (RV stiffness constant between 150 and 250% of normal), systemic cardiac output in 1.5VR exceeds that in 2VR. Although SVC pressure is still higher in 1.5VR than in APC, RAP is lower in 1.5VR than in the other procedures. This condition is favorable to reduce supraventricular arrhythmias related to high RAP during the perioperative periods. This beneficial effect is not expected for 2VR since RAP in 2VR is higher than the atrial pressure of TCPC. Furthermore, 1.5VR is advantageous from the viewpoint of stressed blood volume because 1.5VR needs smaller stressed blood volume than does 2VR to maintain MAP (Fig. 3d).

In these patients, RVEDV in 1.5VR is relatively independent of the RV stiffness constant. However, abnormal systemic venous collateral channels might open after 1.5VR. These collateral channels would increase RV preload wastefully and decrease systemic cardiac output in the late postoperative phase. In such conditions, conversion to the Fontan circulation may be required in the late phase [4, 5]. Nevertheless, 1.5VR should be recommended for the intermediate RV hypoplasia group because high cardiac output and low RAP are anticipated.

Severe RV hypoplasia

When RV hypoplasia is severe (RV stiffness constant >250% of normal), neither 1.5VR and 2VR are expected to improve systemic cardiac output. In this condition, RVEDV is almost the same between 1.5VR and 2VR, and linearly decreases with an increase in the RV stiffness constant in spite of a rapid elevation in RAP. This indicates that RVEDV might be independent of the venous return to RA. Since RAP becomes higher than the atrial pressure of TCPC even in 1.5VR, supraventricular arrhythmias caused by high RAP are liable to occur [2, 5]. In this condition, 1.5VR is considered to have hemodynamics equivalent to APC and needs larger stressed blood volume than does TCPC to maintain systemic arterial pressure (Fig. 3d).

Therefore, TCPC should be chosen for patients with severe RV hypoplasia. In these patients, the arrhythmic events after TCPC are less than that after APC [21, 22]. Although a small pressure gradient between SVC and IVC

remains in 1.5VR, this may not be of clinical significance. Systemic venous collateral channels are expected to be rare, and an increase of RV volume after the operation is unlikely.

Clinical implication

The management strategy for patients with hypoplastic RV has been based on the morphological characteristics, which are dependent on the loading conditions. In contrast, we used a relatively load-independent index, RV stiffness constant, and simulated the postoperative hemodynamics. As a result, we identified the characteristics of hemodynamics after each of the surgical options, and clearly defined the indications of these operations.

Moreover, our results may be useful to theoretically speculate the reason for contrasting clinical findings. Chowdhury and colleagues [2] reported that the event rate of supraventricular arrhythmia was about 15% in the late postoperative phase of 1.5VR. On the other hand, Numata et al. [5] reported higher arrhythmic event rate. In the former report, the patients had a relatively high postoperative RV volume (45–75% of predicted normal RV; Fig. 3c) and a large pressure gradient between SVC and IVC (mean 7.6 mmHg; Fig. 3b) after 1.5VR. Indeed, there was significant pleural effusion in 22.7% of patients. Our results suggest that good systemic cardiac output, low IVC pressure, and high SVC pressure after 1.5VR can be expected under a condition of a relatively small RV stiffness constant. A great difference between SVC and IVC pressures may cause pleural effusion. Therefore, patients in the former report are likely to have low RV stiffness. In the latter report, the average RVEDV at 1 year after 1.5VR was about 50% of normal and there was no obvious collateral after the surgery in the patients examined. These data suggest a high RV stiffness (Fig. 3c), and a small difference between SVC and IVC pressures (Fig. 3b). Since higher arrhythmic event rate is likely to be associated with high RAP in patients with high RV stiffness, we can interpret the marked difference in arrhythmic event rate in these studies based on postoperative hemodynamics. Operations with 1.5 VR in potentially inappropriate patients (i.e., patients with stiffer RV) might impair long-term outcomes by continued high RAP-induced arrhythmia.

If we can assess the RV stiffness constant and other hemodynamic data in a catheter laboratory before operation, we will be able to select the most suitable operation for patients with hypoplastic RV. Recently, noninvasive methods for predicting LV chamber stiffness using echocardiography have been reported [23–25]. For example, LV chamber stiffness has been estimated from the deceleration time of LV early filling, effective mitral area and length. Such a method may be applied to estimate RV chamber stiffness using the deceleration time of RV early filling, effective tricuspid area and length. Moreover, it may be possible to choose an appropriate procedure for individual patients by performing simulation of postoperative hemodynamics from individual data using our model. Further clinical studies are needed to precisely assess the RV stiffness constant, including the above methods.

Limitations

A major limitation of this study is related to the parameters we used for the model. In our model, all parameters other than the RV stiffness constant are fixed. It is reported that RV end-systolic elastance as well as the RV stiffness constant depend upon RV histological changes such as RV hypertrophy [26]. The increase in RV end-systolic elastance moves the beneficial range of 1.5VR toward the stiffer range of the RV stiffness constant. The increase of heart rate also moves the range toward the stiffer range (Table 3). Moreover, ischemia caused by long-standing hypoxemia and hypertension of RV may influence other variables [6]. The existence of pulsatility of the pulmonary circulation may also affect the pulmonary vascular resistance [27]. Tricuspid regurgitation may also impair the postoperative hemodynamics. These limitations may be solved by using the preoperative data of individual patients. Santamore and Burkhoff have already reported the importance of ventricular interdependence using a computer model [13]. However, ventricular interdependence between small hypoplastic RV and relatively large left ventricle may be negligible.

Table 3 The influence of right ventricular end-systolic elastance and heart rate on the beneficial range of the one and a half ventricle repair

	Lower limit of RV stiffness constant (% of normal)	Upper limit of RV stiffness constant (% of normal)
$E_{es,RV}$ = 0.7, HR = 75	150	250
$E_{es,RV}$ = 1.4, HR = 75	200	300
$E_{es,RV}$ = 0.7, HR = 100	175	275

RV Right ventricle, $E_{es,RV}$ right ventricular end-systolic elastance (mmHg/ml), *HR* heart rate (beats/min)

Conclusion

Using a model analysis, we have shown that the beneficial effect of 1.5VR depends on the RV stiffness constant. 1.5VR is the most beneficial for hypoplastic RV with 150–250% of normal RV stiffness constant. The beneficial range of 1.5VR may also be changed by individual parameters other than the RV stiffness constant, but the beneficial range certainly exists. Therefore, determination of management strategy should be based not only on the morphologic parameters but also on the physiologically determined properties.

Acknowledgments This study was supported by Health and Labor Sciences Research Grants (H18-nano-Ippan-003, H19-nano-Ippan-009, H20-katsudo-Shitei-007 and H21-nano-Ippan-005) from the Ministry of Health, Labor and Welfare of Japan, by Grants-in-Aid for Scientific Research (No. 20390462) from the Ministry of Education, Culture, Sports, Science and Technology in Japan, and by the Industrial Technology Research Grant Program from New Energy and Industrial Technology Development Organization (NEDO) of Japan.

References

1. Yoshimura N, Yamaguchi M, Ohashi H, Oshima Y, Oka S, Yoshida M, Murakami H, Tei T (2003) Pulmonary atresia with intact ventricular septum: strategy based on right ventricular morphology. J Thorac Cardiovasc Surg 126:1417–1426
2. Chowdhury UK, Airan B, Talwar S, Kothari SS, Saxena A, Singh R, Subramaniam GK, Juneja R, Pradeep KK, Sathia S, Venugopal P (2005) One and one-half ventricle repair: results and concerns. Ann Thorac Surg 80:2293–2300
3. Hanley FL (1999) The one and a half ventricle repair-we can do it, but should we do it? J Thorac Cardiovasc Surg 117:659–661
4. Uemura H, Yagihara T, Adachi I, Kagisaki K, Shikata F (2007) Conversion to total cavopulmonary connection after failed one and one-half ventricular repair. Ann Thorac Surg 84:666–668
5. Numata S, Uemura H, Yagihara T, Kagisaki K, Takahashi M, Ohuchi H (2003) Long-term functional results of the one and one half ventricular repair for the spectrum of patients with pulmonary atresia/stenosis with intact ventricular septum. Eur J Cardiothorac Surg 24:516–520
6. Freedom RM (1998) Pulmonary atresia with intact ventricular septum—the significance of the coronary arterial circulation. In: Redington AN, Brawn WJ, Deanfield JE, Anderson RH (eds) The right heart in congenital heart disease. Greenwich Medical Media, London
7. Hanley FL, Sade RM, Blackstone EH, Kirklin JW, Freedom RM, Nanda NC (1993) Outcomes in neonatal pulmonary atresia with intact ventricular septum. A multiinstitutional study. J Thorac Cardiovasc Surg 105:406–427
8. Ashburn DA, Blackstone EH, Wells WJ, Jonas RA, Pigula FA, Manning PB, Lofland GK, Williams WG, McCrindle BW, Congenital Heart Surgeons Study members (2004) Determinants of mortality and type of repair in neonates with pulmonary atresia and intact ventricular septum. J Thorac Cardiovasc Surg 127:1000–1007
9. Burkhoff D, Tyberg JV (1993) Why does pulmonary venous pressure rise after onset of LV dysfunction: a theoretical analysis. Am J Physiol 265:H1819–H1828
10. Morley D, Litwak K, Ferber P, Spence P, Dowling R, Meyns B, Griffith B, Burkhoff D (2007) Hemodynamic effects of partial ventricular support in chronic heart failure: results of simulation validated with in vivo data. J Thorac Cardiovasc Surg 133:21–28
11. Goodwin JA, van Meurs WL, Sá Couto CD, Beneken JE, Graves SA (2004) A model for educational simulation of infant cardiovascular physiology. Anesth Analg 99:1655–1664
12. Migliavacca F, Pennati G, Dubini G, Fumero R, Pietrabissa R, Urcelay G, Bove EL, Hsia TY, de Leval MR (2001) Modeling of the Norwood circulation: effects of shunt size, vascular resistances, and heart rate. Am J Physiol Heart Circ Physiol 280:H2076–H2086
13. Santamore WP, Burkhoff D (1991) Hemodynamic consequences of ventricular interaction as assessed by model analysis. Am J Physiol 260:H146–H157
14. Sagawa K, Maughan L, Suga H, Sunagawa K (1988) Cardiovascular interaction. In: Sagawa K, Maughan L, Suga H, Sunagawa K (eds) Cardiac contraction and the pressure–volume relationship. Oxford University Press, Oxford
15. Walther FJ, Siassi B, King J, Wu PY (1986) Blood flow in the ascending and descending aorta in term newborn infants. Early Hum Dev 13:21–25
16. Wang JJ, Flewitt JA, Shrive NG, Parker KH, Tyberg JV (2006) Systemic venous circulation. Waves propagating on a windkessel: relation of arterial and venous windkessels to systemic vascular resistance. Am J Physiol Heart Circ Physiol 290:H154–H162
17. McElhinney DB, Reddy VM, Hanley FL, Moore P (1997) Systemic venous collateral channels causing desaturation after bidirectional cavopulmonary anastomosis: evaluation and management. J Am Coll Cardiol 30:817–824
18. Gatzoulis MA, Shinebourne EA, Redington AN, Rigby ML, Ho SY, Shore DF (1995) Increasing cyanosis early after cavopulmonary connection caused by abnormal systemic venous channels. Br Heart J 73:182–186
19. Webber SA, Horvath P, LeBlanc JG, Slavik Z, Lamb RK, Monro JL, Reich O, Hruda J, Sandor GG, Keeton BR, Salmon AP (1995) Influence of competitive pulmonary blood flow on the bidirectional superior cavopulmonary shunt. A multi-institutional study. Circulation 92:II279–II286
20. Trusler GA, Williams WG, Cohen AJ, Rabinovitch M, Moes CA, Smallhorn JF, Coles JG, Lightfoot NE, Freedom RM (1990) William Glenn lecture. The cavopulmonary shunt. Evolution of a concept. Circulation 82:IV131–IV138
21. Gelatt M, Hamilton RM, McCrindle BW, Gow RM, Williams WG, Trusler GA, Freedom RM (1994) Risk factors for atrial tachyarrhythmias after the Fontan operation. J Am Coll Cardiol 24:1735–1741
22. Balaji S, Gewillig M, Bull C, de Leval MR, Deanfield JE (1991) Arrhythmias after the Fontan procedure. Comparison of total cavopulmonary connection and atriopulmonary connection. Circulation 84:III162–III167
23. Little WC, Ohno M, Kitzman DW, Thomas JD, Cheng CP (1995) Determination of left ventricular chamber stiffness from the time for deceleration of early left ventricular filling. Circulation 92:1933–1939
24. Lisauskas JB, Singh J, Bowman AW, Kovács SJ (2001) Chamber properties from transmitral flow: prediction of average and passive left ventricular diastolic stiffness. J Appl Physiol 91:154–162
25. Garcia MJ, Firstenberg MS, Greenberg NL, Smedira N, Rodriguez L, Prior D, Thomas JD (2001) Estimation of left ventricular operating stiffness from Doppler early filling deceleration time in humans. Am J Physiol Heart Circ Physiol 280:H554–H561
26. Gaynor SL, Maniar HS, Bloch JB, Steendijk P, Moon MR (2005) Right atrial and ventricular adaptation to chronic right ventricular pressure overload. Circulation 112:I212–I218
27. Szabó G, Buhmann V, Graf A, Melnitschuk S, Bährle S, Vahl CF, Hagl S (2003) Ventricular energetics after the Fontan operation: contractility-afterload mismatch. J Thorac Cardiovasc Surg 125:1061–1069

J Physiol 589.7 (2011) pp 1769–1790

The Journal of Physiology

Closed-loop spontaneous baroreflex transfer function is inappropriate for system identification of neural arc but partly accurate for peripheral arc: predictability analysis

Atsunori Kamiya, Toru Kawada, Shuji Shimizu and Masaru Sugimachi

Department of Cardiovascular Dynamics, National Cerebral and Cardiovascular Center Research Institute, Suita-city, Osaka 565-8565, Japan

Non-technical summary The arterial baroreflex is a closed-loop, negative feedback control system that senses baroreceptor pressure and controls systemic arterial pressure (AP) to attenuate perturbations in AP. The total arc of the baroreflex consists of two subsystems: the neural (baroreceptor pressure input to sympathetic nerve activity (SNA)) and peripheral (SNA input to AP) arcs. We show that although the spontaneous baroreflex transfer function obtained by closed-loop analysis has been believed to represent the neural arc function, it is inappropriate for system identification of the neural arc but is essentially appropriate for the peripheral arc under resting condition, when compared with open-loop transfer functions that have good predictabilities of time-series output dynamics from input signals. Our results indicate that in the spontaneous baroreflex system under closed-loop conditions, the peripheral arc (feedforward) function predominates over the neural arc (feedback) function, probably because of the SNA component that is independent of the baroreceptor pressure input.

Abstract Although the dynamic characteristics of the baroreflex system have been described by baroreflex transfer functions obtained from open-loop analysis, the predictability of time-series output dynamics from input signals, which should confirm the accuracy of system identification, remains to be elucidated. Moreover, despite theoretical concerns over closed-loop system identification, the accuracy and the predictability of the closed-loop spontaneous baroreflex transfer function have not been evaluated compared with the open-loop transfer function. Using urethane and α-chloralose anaesthetized, vagotomized and aortic-denervated rabbits ($n = 10$), we identified open-loop baroreflex transfer functions by recording renal sympathetic nerve activity (SNA) while varying the vascularly isolated intracarotid sinus pressure (CSP) according to a binary random (white-noise) sequence (operating pressure $\pm$ 20 mmHg), and using a simplified equation to calculate closed-loop-spontaneous baroreflex transfer function while matching CSP with systemic arterial pressure (AP). Our results showed that the open-loop baroreflex transfer functions for the neural and peripheral arcs predicted the time-series SNA and AP outputs from measured CSP and SNA inputs, with r^2 of 0.8 ± 0.1 and 0.8 ± 0.1, respectively. In contrast, the closed-loop-spontaneous baroreflex transfer function for the neural arc was markedly different from the open-loop transfer function (enhanced gain increase and a phase lead), and did not predict the time-series SNA dynamics (r^2; 0.1 ± 0.1). However, the closed-loop-spontaneous baroreflex transfer function of the peripheral arc partially matched the open-loop transfer function in gain and phase functions, and had limited but reasonable predictability of the time-series AP dynamics (r^2, 0.7 ± 0.1). A numerical simulation suggested that a noise predominantly in the neural arc under resting conditions might be a possible mechanism responsible for our findings. Furthermore, the predictabilities of the neural arc transfer functions obtained in open-loop and closed-loop conditions were validated by closed-loop pharmacological (phenylephrine and nitroprusside infusions) pressure interventions. Time-series SNA responses

DOI: 10.1113/jphysiol.2011.203455

to drug-induced AP changes predicted by the open-loop transfer function matched closely the measured responses (r^2, 0.9 ± 0.1), whereas SNA responses predicted by closed-loop-spontaneous transfer function deviated greatly and were the inverse of measured responses (r, -0.8 ± 0.2). These results indicate that although the spontaneous baroreflex transfer function obtained by closed-loop analysis has been believed to represent the neural arc function, it is inappropriate for system identification of the neural arc but is essentially appropriate for the peripheral arc under resting conditions, when compared with open-loop analysis.

(Resubmitted 2 December 2010; accepted after revision 7 February 2011; first published online 14 February 2011)
Corresponding author A. Kamiya: Department of Cardiovascular Dynamics, National Cerebral and Cardiovascular Center Research Institute, 5-7-1 Fujishirodai, Suita, Osaka 565-8565, Japan. Email: kamiya@ri.ncvc.go.jp

Abbreviations AP, arterial pressure; CSP, intra-carotid sinus pressure; *r*linear correlation coefficient; RMS, root mean square; SNA, sympathetic nerve activity.

Introduction

The arterial baroreflex plays a crucial role in circulatory control by its dynamic system characteristics (Eckberg & Sleight, 1992; Rowell, 1993). The baroreflex is a closed-loop, negative feedback control system that constantly senses arterial pressure (AP) by baroreceptors and quickly regulates systemic AP physiologically to attenuate perturbations in AP (Eckberg & Sleight, 1992; Rowell, 1993). The total arc baroreflex system consists of two subsystems: the neural and peripheral arcs (Kamiya *et al.* 2005*b*, 2008*a*, 2010; Kawada *et al.* 2010). The neural arc subsystem represents central processing from baroreceptor pressure to efferent sympathetic nerve activity (SNA), whereas the peripheral arc subsystem represents processing from SNA to systemic AP via peripheral circulatory organs including heart, kidney and blood vessels (Fig. 1) (Ikeda *et al.* 1996; Kamiya *et al.* 2005*b*).

Transfer function analysis is a powerful tool to determine the dynamic characteristics of biosystems. This analysis has revealed the dynamic causality mainly in 'open-loop' biosystems, including cerebral autoregulation (Zhang *et al.* 2002), renal vascular function (DiBona & Sawin, 2003, 2004), heart rate control (Ikeda *et al.* 1995) and cutaneous circulation (Kamiya *et al.* 2008*b*). We have applied the transfer function analysis to characterize the 'closed-loop' arterial baroreflex system, in which we used the open-loop and white-noise pressure perturbation techniques to overcome the difficulties of closed-loop system identification (see Appendix A) (Ikeda *et al.* 1996; Kawada *et al.* 2002; Kamiya *et al.* 2005*b*, 2008*a*). We have reported that the neural arc transfer function (H_n) has derivative and high-cut filter characteristics with a pure delay, indicating that more rapid change of arterial pressure results in greater response of SNA to pressure change (Kawada *et al.* 2002; Kamiya *et al.* 2005*b*), whereas the peripheral arc transfer function (H_p) has second-order low-pass filter characteristics with a pure delay (see Appendix B) (Kawada *et al.* 2002; Kamiya *et al.* 2005*b*). However, at least two important issues remain to be elucidated.

First, a hallmark of the transfer function, the predictability of time-series output dynamics from input signals (Ikeda *et al.* 1995; Kamiya *et al.* 2008*b*), has not yet been investigated in the baroreflex system. Accurate system identification of the transfer function yields good predictability, whereas inappropriate system identification results in poor predictability. In the present study, we tested the first hypothesis that the open-loop baroreflex transfer functions of the neural and peripheral arcs are capable of predicting time-series SNA and AP output dynamics from baroreceptor pressure and SNA inputs, respectively.

Second, identifying transfer functions is theoretically difficult under closed-loop and spontaneous resting baroreflex conditions. The reason is that unknown noises in the neural and peripheral arcs would interfere with the accuracy of system identification in closed-loop-spontaneous conditions, in contrast to open-loop transfer function identification where the interfering effects of noises would be eliminated by the open-loop and white-noise pressure perturbation techniques (Ikeda *et al.* 1996; Kawada *et al.* 2002; Kamiya *et al.* 2005*b*, 2008*a*) (see Appendix A). Although earlier interesting studies have applied a simplified (open-loop-like) calculation of transfer function to closed-loop-spontaneous resting baroreflex condition in humans (Cooke *et al.* 1999, 2009; Ogoh *et al.* 2009) and animals (Orea *et al.* 2007) without opening the loop, whether the reported transfer functions are actually capable of predicting time-series output dynamics has not been verified. In addition, the accuracy and limitation of closed-loop-spontaneous baroreflex transfer functions remain unclear from the viewpoint of comparing with open-loop transfer functions. In the present study, we tested the second hypothesis that the closed-loop-spontaneous baroreflex transfer function is limited to predict baroreflex dynamics compared with the open-loop transfer function.

In the present study, by artificially controlling intra-carotid sinus pressure (CSP) and recording renal SNA and systemic AP, we identified the open-loop baroreflex transfer functions by introducing CSP perturbation according to a binary random (white-noise) sequence. We also determined the closed-loop-spontaneous baroreflex transfer functions by matching CSP with systemic AP. We then compared the characteristics and predictability of these transfer functions. Our results confirmed good predictability of the open-loop baroreflex transfer functions, and unexpectedly indicated that the closed-loop-spontaneous transfer function approximately matched the open-loop transfer function for the peripheral arc but deviated markedly from the open-loop transfer function for the neural arc. Thus, the closed-loop-spontaneous baroreflex transfer function is inappropriate for system identification of the neural arc but is partially appropriate for the peripheral arc under resting condition, compared with the open-loop analysis. These findings may have great impact, because the closed-loop-spontaneous baroreflex transfer function has been believed to represent the neural arc function (Orea *et al.* 2007; Cooke *et al.* 2009; Ogoh *et al.* 2009).

Methods

Animal preparation

Animals were cared for in strict accordance with the Guiding Principles for the Care and Use of Animals in the Field of Physiological Science approved by the Physiological Society of Japan and the National Cerebral and Cardiovascular Center Research Institute, and the ethical regulations and policies of *The Journal of Physiology* (Drummond, 2009). Ten Japanese white rabbits weighing 2.4–3.3 kg were initially anaesthetized by intravenous injection (2 ml kg^{-1}) of a mixture of urethane (250 mg ml^{-1}) and α-chloralose (40 mg ml^{-1}). Anaesthesia was maintained by continuously infusing the anaesthetics at a rate of 0.33 ml kg^{-1} h^{-1} using a syringe pump (CFV-3200, Nihon Kohden, Tokyo). The rabbits

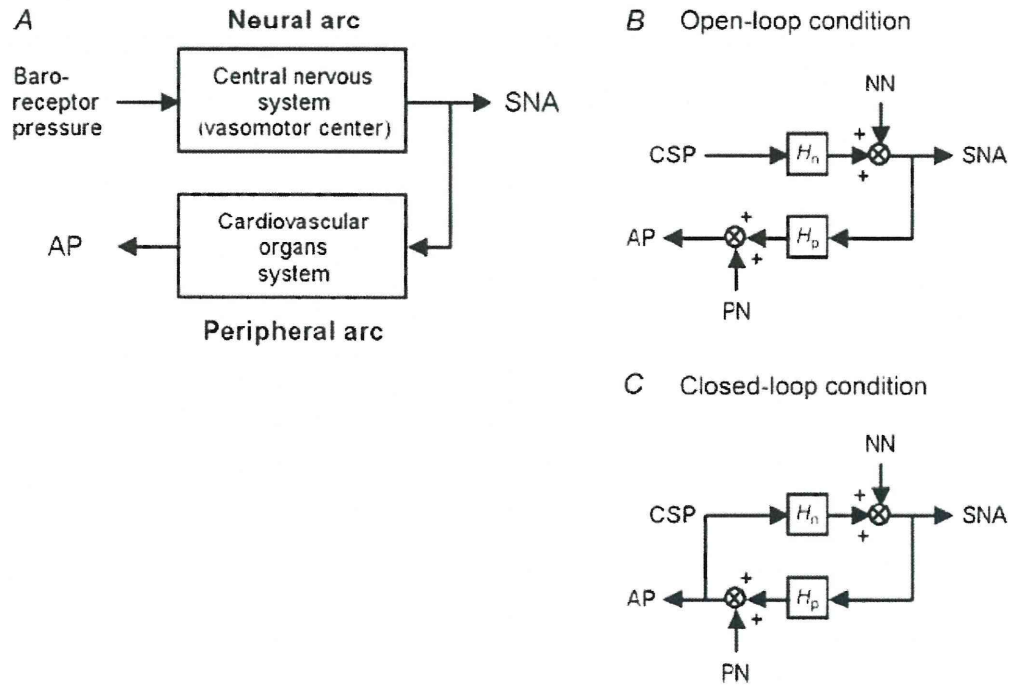

Figure 1. Functional structure of arterial baroreflex system
A, theoretical considerations of the coupling of baroreflex neural and peripheral arcs. Although baroreflex is a negative feedback control system that senses AP by baroreceptors and regulates AP, we opened the loop by changing baroreceptor pressure independent of AP. By measuring SNA, we divided the baroreflex system into the neural arc (from baroreceptor pressure input to efferent SNA via central nervous system) and the peripheral arc (from SNA input to AP via cardiovascular organs system). *B*, block diagram of open-loop baroreflex system. Because of vascular isolation of carotid-sinus regions, CSP is independent of systemic AP. Noise is introduced to the neural and/or peripheral arcs. *C*, block diagram of closed-loop-spontaneous baroreflex system, where CSP equals AP. Noise is introduced to the neural and/or peripheral arcs. Because of the closed-loop nature, changes in AP (and thus, in CSP) control SNA via neural arc transfer function (H_n), which in turn modulate AP via peripheral arc transfer function (H_p). CSP, carotid sinus pressure; SNA, sympathetic nerve activity; AP, arterial pressure; NN, unknown noise in the neural arc; PN, unknown noise in the peripheral arc.

were mechanically ventilated with oxygen-enriched room air. Bilateral carotid sinuses were isolated vascularly from the systemic circulation by ligating the internal and external carotid arteries and other small branches originating from the carotid sinus regions. The isolated carotid sinuses were filled with warmed physiological saline pre-equilibrated with atmospheric air, through catheters inserted via the common carotid arteries. CSP was controlled by a servo-controlled piston pump (model ET-126A, Labworks; Costa Mesa, CA, USA). Bilateral vagal and aortic depressor nerves were sectioned in the middle of the neck region to eliminate reflexes from the cardiopulmonary region and the aortic arch. Systemic AP was measured using a high-fidelity pressure transducer (Millar Instruments; Houston, TX, USA) inserted retrograde from the right common carotid artery below the isolated carotid sinus region. A catheter was inserted into the right femoral vein to infuse phenylephrine and nitroprusside. Body temperature was maintained at around 38 °C with a heating pad.

The left renal sympathetic nerve was exposed retroperitoneally. A pair of stainless steel wire electrodes (Bioflex wire AS633, Cooner Wire) was attached to the nerve to record renal SNA. The nerve fibres peripheral to the electrodes were ligated tightly and crushed to eliminate afferent signals. The nerve and electrodes were covered with a mixture of silicone gel (Silicon Low Viscosity, KWIK-SIL, World Precision Instrument, Inc., FL, USA) to insulate and immobilize the electrodes. The pre-amplified SNA signal was band-pass filtered at 150–1000 Hz. These nerve signals were full-wave rectified and low-pass filtered with a cut-off frequency of 30 Hz to quantify the nerve activity.

Protocols

After the surgical preparation, all animals ($n = 10$) were maintained supine. The overall scheme of the experimental design is shown in Fig. 2. Protocols 1–4 were conducted in randomized order at intervals of at least 5 min, while protocol 5 was done finally. In all protocols, bilateral CSP was controlled by a servo-controlled piston pump (Kawada *et al.* 2002). The SNA, CSP and AP were recorded at a sampling rate of 200 Hz using a 12-bit analog-to-digital converter. Data were stored on the hard disk of a dedicated laboratory computer system.

Before these protocols, operating AP and SNA in baroreflex closed-loop condition were determined. First, CSP was matched with systemic AP to close the baroreflex loop. After at least 5 min of stabilization, the variables were recorded for 10 min, and the average AP over 10 min was defined as the operating AP under closed-loop condition.

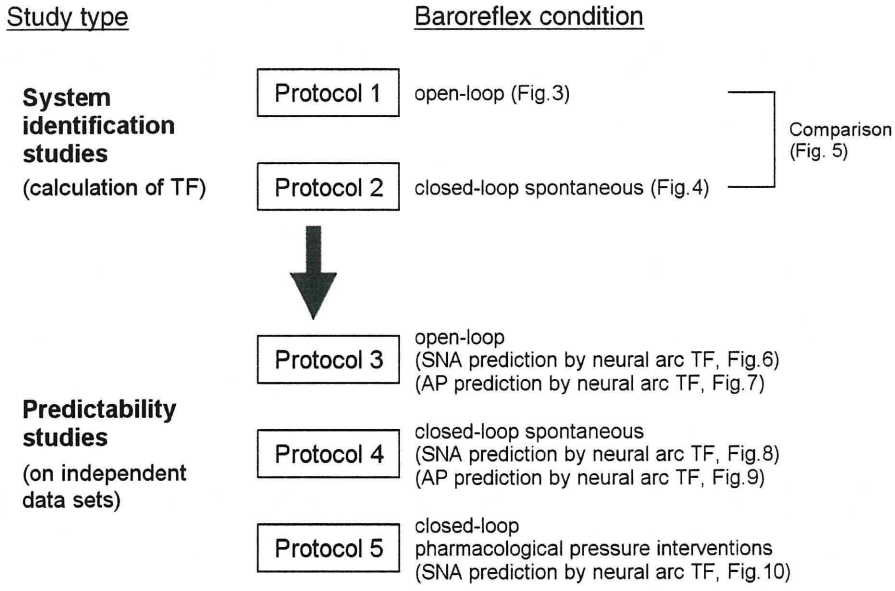

Figure 2. Experimental design
In system identification studies, open-loop (protocol 1, CSP was perturbed according to a binary random sequence) and closed-loop-spontaneous (protocol 2, CSP was matched with systemic AP) baroreflex transfer functions were identified from experimental data. In predictability studies, the predictive power of the above transfer functions was tested using independent data (protocols 3, 4 and 5). Protocol 3 and 4 were open-loop and closed-loop-spontaneous baroreflex conditions, respectively. Protocol 5 was pharmacological pressure intervention by phenylephrine and nitroprusside infusions in closed-loop condition. TF, transfer function; CSP, carotid sinus pressure; SNA, sympathetic nerve activity; AP, arterial pressure.

System identification studies. Protocol 1 was performed to identify the open-loop baroreflex transfer functions. After at least 5 min of stabilization, CSP was randomly assigned at 20 mmHg above or below the operating AP every 500 ms according to a binary random (white-noise) sequence, in which the input power spectrum of CSP was reasonably flat up to 1 Hz (Kawada *et al.* 2002). The variables were recorded for 10 min and stored for analysis.

Protocol 2 was performed to determine the closed-loop-spontaneous baroreflex transfer functions by a convenient method of applying the same calculation as that used in the open-loop condition of protocol 1 (see Appendix A). CSP was matched with systemic AP to close the baroreflex loop. After at least 5 min of stabilization, the variables were recorded for 10 min and stored for analysis.

Predictability studies. Protocols 3, 4 and 5 were performed to investigate the predictability of baroreflex transfer functions. In protocol 3 (open-loop), CSP was randomly assigned at 20 mmHg above or below the operating AP. The variables were recorded for 10 min and stored for analysis.

In protocol 4 (closed-loop), CSP was matched with systemic AP to close the baroreflex loop. After at least 5 min of stabilization, the variables were recorded for at least 10 min and stored for analysis.

Protocol 5 was also performed to investigate the predictability of baroreflex transfer functions during sequential pharmacological pressure interventions in the closed-loop condition. CSP was matched with systemic AP. After at least 2 min of stabilization, phenylephrine hydrochloride ($3\ \mu g\ kg^{-1}$) was bolus infused through a venous catheter inserted into the right femoral vein, followed 1–2 min later by sodium nitroprusside ($4\ \mu g\ kg^{-1}$) and then 1–2 min later by the second phenylephrine hydrochloride infusion ($4\ \mu g\ kg^{-1}$). The variables were recorded continuously for at least 10–11 min and stored for analysis.

Data analysis

SNA signal was normalized by the following steps. First, 0 arbitrary unit (a.u.) was assigned to the post-mortem noise level. Second, 100 a.u. was assigned to the SNA signals averaged over 10 min before protocols. Last, the other SNA signals in protocols 1–5 were then normalized to these values.

In protocol 1, we calculated the open-loop transfer (gain and phase) and coherence functions from CSP input to SNA in the neural arc ($H_{\text{n-open}}$) and from SNA to AP in the peripheral arc ($H_{\text{p-open}}$). We re-sampled CSP and SNA at 10 Hz and segmented them into 10 sets of 50% overlapping bins of 2^{10} data point each. The segment length was 102.4 s, which yielded the lowest frequency bound of 0.01 (0.0097) Hz. We subtracted a linear trend and applied a Hanning window for each segment. We then performed fast Fourier transform to obtain frequency spectra of input (x) and output (y). The inputs are CSP and SNA, while the outputs are SNA and AP in the neural and peripheral arc subsystems, respectively. We ensemble averaged the input power ($Sxx(f)$), output power ($Syy(f)$), and cross power between input and output ($Syx(f)$) over the 10 segments. Then, we calculated the transfer function ($H(f)$) from input to output as follows:

$$H(f) = \frac{Syx(f)}{Sxx(f)} \tag{1}$$

Although individual noise may be present in the neural and peripheral arc subsystems, the effects of noise on the calculations of transfer functions are eliminated by open-loop operation and white-noise-like perturbation of CSP (see Appendix A, Fig. 1*A*).

To quantify the linear dependence between input and output in the frequency domain, we calculated the magnitude-squared coherence function ($\text{Coh}(f)$) as follows:

$$\text{Coh}(f) = \frac{|Syx(f)|^2}{Sxx(f)Syy(f)} \tag{2}$$

The coherence values range from zero to unity. Unity coherence indicates a perfect linear dependence between input and output, whereas zero coherence indicates total independence of these two signals. To quantify the errors on individual gain and phase estimates, we calculated the normalized random error ($\varepsilon(f)$) as follows:

$$\varepsilon(f) = \sqrt{\frac{1 - \text{Coh}(f)}{2n_{\text{d}}\text{Coh}(f)}} \tag{3}$$

where n_{d} is the number of distinct subrecord, when the error in gain factor estimate matches that in phase factor estimate (Julius & Allan, 2000).

To quantify the transfer characteristics in the time domain, step response was calculated by discrete from convolution integral as follows:

$$Y(t) = \sum_{\tau=0}^{N} h(\tau) \cdot X(t-\tau) \tag{4}$$

where $h(\tau)$ is the impulse response obtained by inverse fast Fourier transform of the transfer function ($H(f)$); N is the total number of data elements; τ is the convolution parameter; t is time in increments of 0.1 s (or 10 Hz); $X(t) = 0$ for $t < 0$ and $X(t) = 1$ for $t \geq 0$.

It should be noted that since protocol 2 was a closed-loop and spontaneous baroreflex condition, unknown noise, if present in the neural and peripheral arc subsystems, would affect the accuracy of system identification (see Appendix A, Fig. 1*B*). Based on earlier

studies (Cooke *et al.* 1999, 2009; Ogoh *et al.* 2009), we applied a simplified (open-loop-like) calculation of transfer function to the closed-loop-spontaneous resting baroreflex condition, and estimated the closed-loop-spontaneous baroreflex transfer functions from AP input to SNA in the neural arc ($H_{\text{n-closed-spon}}$) and from SNA to AP in the peripheral arc ($H_{\text{p-closed-spon}}$), together with coherence functions and step responses (see Appendix A).

In protocols 3 and 4, we calculated the predicted time-series output dynamics (SNA and AP) from measured input signals (CSP/AP and SNA in the neural and peripheral arc, respectively), using eqn (4) and impulse response obtained from the transfer functions in protocols 1 and 2. The predicted output was scatter-plotted, and compared with the actually measured output by calculating the linear correlation coefficient (r) and root mean square (RMS). The analysis was performed using the data at arbitrarily selected 1 and 3 min in protocols 3 and 4, respectively.

In protocol 5, similar to protocol 3 and 4, we calculated the predicted time-series output dynamics of SNA from measured pressure input signals (CSP/AP in the neural arc) during pharmacological interventions. The predicted SNA was scatter-plotted, and compared with the actual SNA measurements by calculating r and RMS. The analysis was performed using the data for 10–11 min. Since AP was determined by interventions (phenylephrine and nitroprusside infusions) and not by SNA, we did not calculate the predicted AP dynamics from the measured SNA signals.

Statistic analysis

All data are presented as means ± SD. Paired t test and repeated measures analysis of variance with *post hoc* multiple comparisons were used to compare variables as appropriate. Differences were considered significant when $P < 0.05$.

Results

Open-loop transfer function (protocol 2)

Figure 3 shows a typical example of the open-loop system identification of baroreflex transfer functions in protocol 2. CSP was perturbed according to a binary random (white-noise) sequence at 500 ms intervals (Fig. 3*A*, green line). When CSP was increased, SNA decreased, and vice versa. In the frequency domain, the input power spectrum of CSP was reasonably flat up to 1 Hz (Fig. 3*B*, green line).

The open-loop transfer function of the neural arc from CSP input to SNA ($H_{\text{n-open}}$; Fig. 3*C*, left panels) showed that the gain increased as the frequency of CSP perturbation increased between 0.01 Hz and 0.4 Hz, indicating dynamic high-pass characteristics. The phase approached $-\pi$ at the lowest frequency, indicating a negative SNA response to CSP changes, and lagged as the frequency increased (Fig. 3*C*, left panels). The coherence was over 0.8 between 0.03 to 0.4 Hz except at around 0.35 Hz (Fig. 3*C*, left panels). The step response (Fig. 3*D*, left panel) of SNA in response to CSP consisted of an initial decrease followed by partial recovery and then steady state.

The open-loop transfer function of the peripheral arc from SNA input to AP ($H_{\text{p-open}}$, Fig. 3*C*, right panels) showed that the gain decreased as the frequency increased, indicating low-pass characteristics. The phase approached zero at the lowest frequency, indicating a positive AP response to SNA changes, and lagged as the frequency increased. The coherence was over 0.8 between 0.01 to 0.3 Hz except at around 0.2 Hz (Fig. 3*C*, right panels). The step response (Fig. 3*D*, right panel) of SNA to CSP was a gradual increase to steady state.

The transfer function of baroreflex total arc from CSP input to systemic AP identified in the open-loop condition (Fig. 3*E*) showed that the gain decreased as the frequency increased, indicating low-pass characteristics that were milder than $H_{\text{p-open}}$. The phase approached $-\pi$ at the lowest frequency, indicating negative feedback system characteristics of baroreflex (negative AP response to CSP changes). The phase lagged as frequency increased. The transfer function of total arc was almost consistent with multiplication of tandemly arranged open-loop transfer functions of neural ($H_{\text{n-open}}$) and peripheral ($H_{\text{p-open}}$) arcs (Fig. 1*A* and *B*), at the frequency where their coherence functions were high.

Closed-loop-spontaneous transfer function (protocol 3)

Figure 4 shows a typical example of the closed-loop-spontaneous transfer functions simplified, calculated in protocol 3 by applying open-loop-like calculations to closed-loop-spontaneous data. The data were obtained from the same animal as in Fig. 3.

We closed the baroreflex loop by matching CSP with systemic AP. The exact match of the two parameters was demonstrated by autospectrum (Fig. 4*B*) and beat-to-beat waveform (Fig. 4*C*), both showing overlapping of CSP (green line) and systemic AP (black line). The exact match was further confirmed by the transfer functions from CSP to systemic AP (Fig. 4*D*), which showed that the gain, phase and coherence functions were maintained constant at 1, zero and 1, respectively.

The closed-loop-spontaneous transfer function of the neural arc ($H_{\text{n-closed-spon}}$) from CSP (that equalled AP) to SNA (Fig. 4*E*, left panels, black line) was markedly different from the open-loop transfer function ($H_{\text{n-open}}$, red line) with respect to gain, phase, coherence and step response. The increase in gain *versus* frequency was